

Probing flavor changing interactions in hadron collisions *

Chang Chao-Hsi^{a,b}, Han Liang^c, Jiang Yi^c, Ma Wen-Gan^{a,b,c}, Zhou Hong^c, Zhou Mian-Lai^c

^aCCAST (World Laboratory), P.O.Box 8730, Beijing 100080, China.

^bInstitute of Theoretical Physics, Academia Sinica,
P.O.Box 2735, Beijing 100080, China.

^cDepartment of Modern Physics, University of Science and Technology
of China (USTC), Hefei, Anhui 230027, China.

Abstract

The subprocess $gg \rightarrow t\bar{c} + \bar{t}c$ in the two-Higgs-doublet model with flavor-changing scalar couplings is examined at the one loop level. With perturbative QCD factorization theorem, the corresponding cross sections for hadron-hadron collisions are computed numerically. The results are applicable to the whole mass range of the weakly coupled Higgs bosons. In case we could efficiently exclude the severe backgrounds of the $t\bar{c}(\bar{t}c)$ production signal, probing the flavor-changing top-charm-scalar vertex at hadron colliders would be very promising and accessible experimentally.

PACS number(s):13.85.Ni, 11.30.Hv, 12.60.Fr,
14.65.Ha

*This work was supported by National Natural Science Foundation of China.

I. Introduction

There are stringent experimental constraints against the existence of tree level neutral flavor changing interactions, especially for light quarks[1]. This leads to the naturalness to suppress the flavor changing neutral current interactions (FCNCs) for all kinds of model building studies, that is realized in terms of the Glashow-Iliopoulos-Maiani (GIM) mechanism in the standard model(SM).

The two-Higgs-doublet models(THDMs) are extensions of the SM in which one more scalar doublet is added. In order to forbid possible tree level FCNCs to appear in the models, Glashow and Weinberg[3] proposed a neutral flavor conservation (NFC) condition by imposing discrete symmetries on the models. The common THDMs with the NFC condition can be divided into two categories, i.e., Model I and Model II. In Model I, both the up- and down-type quarks couple to the same one of the Higgs doublets, but in the Model II the up- and down-type quarks couple to the two Higgs doublets respectively. In fact, the suppression facts of the FCNC processes in the cases involving the light down-type quark sector have been observed experimentally[4], whereas those relevant to the up-type quark sector have not been established so well. Therefore the so-called Model-III of the THDM is proposed and it allows the FCNC Yukawa couplings which has the character that the couplings are related to the masses of the coupled flavors even at tree level[2].

As pointed out by Cheng, Sher and other authors[6][7] [8][9], the Yukawa couplings are typically proportional to the masses of the coupled fermions at the vertices, it is rather natural to imagine having such Yukawa couplings for the FCNC interactions instead of placing the constraints on the theory. In this case, low energy limits on the FCNCs may be evaded, because the flavor changing couplings to the light quarks are small, and the suppression of the FCNC processes involving light quarks can be automatically satisfied. Then the imposition of discrete symmetries to obtain the NFC condition, therefore, is unnecessary, which is normally invoked in common THDMs to prevent the FCNC interactions at tree level. In the literature such the THDM without the NFC condition is called as the ‘third’ THDM (i.e., THDM III) [9], where the up-type and down-type quarks are allowed simultaneously to couple to more than one scalar doublet. In the framework of the model the effects of the FCNC interactions involving the heavy quark will be enhanced.

Now the top quark has been observed and a unexpected very large mass $m_t = 173.8 \pm 5.2 \text{ GeV}$ (world average value) has been recognized[5]. This ‘extraordinary’ mass scale of the top quark may have many important implications pertaining to many outstanding issues. One of them is to test the FCNC processes requested in the Model-III. Namely, it is a ‘good place’ to observe the facts of the Model-III for the FCNC interactions. The measurement of FCNC processes involving top quark would provide an important test for the discrimination of various models. In the THDM III one would expect that large effects of the FCNC interactions could manifest themselves in the cases involving the massive top quark. Therefore testing the existence of the flavor changing scalar interactions involving top quarks are clearly important. D. Atwood et al. [10] presented results of a calculation for the process $e^+e^- \rightarrow t\bar{c}$ (or $\bar{t}c$)in the THDM III, and they obtained R^{tc}/λ^4 to be in the order of 10^{-5} with proper parameters. Recently, Jiang et al.[11]studied the production rates of $e^+e^- \rightarrow \gamma\gamma \rightarrow t\bar{c} + \bar{t}c$ for the NLC and found that this process is more promising than the straight production via e^+e^- collisions for probing the FCNC interactions. Abraham et al.[12] also

investigated the anomalous $\bar{t}q\gamma$ couplings via single top quark production processes by considering effective Lagrangian of the lowest dimension with $\gamma\gamma$ collisions, and found the processes would be observable with suitable strength of anomalous coupling as long as b-tagging and suitable kinematic cuts are taken properly.

After the termination of the running of the LEP2, the hadron colliders Tevatron and LHC will be the only machines in searching for the FCNC processes. It is believed that more experimental events involving top quark will be collected in these hadronic machines. It will give a good chance to study the physics relevant to the FCNC processes of the Model-III. In this paper we are to study the problem and present complete one-loop calculation for the subprocess $gg \rightarrow t\bar{c}$ (or $\bar{t}c$) to the order $O(m_t m_c/m_W^2)$ for the THDM Model-III. In fact, the obtained results in the paper are applicable to the whole mass range for weakly coupled Higgs bosons. The production cross sections of $pp(\bar{p}) \rightarrow gg \rightarrow t\bar{c} + \bar{t}c + X$ are also given for the Tevatron and LHC. The paper is organized as follows: The details of the calculation are given in Sec. II. In Sec. III numerical results, discussions and a short summary are presented. Finally, the explicit expressions used in the paper are collected in appendix.

II. Calculation

In the third type of the two-Higgs-doublet model, the up-type and down-type quarks are allowed simultaneously to couple to more than one scalar doublet. Since there is no global symmetry that distinguishes the two doublets in the model, we will assume that only one of them (ϕ_1) develops a vacuum expectation value and the second one (ϕ_2) remains unbroken, i.e.

$$\langle \phi_1 \rangle = \begin{pmatrix} 0 \\ v/\sqrt{2} \end{pmatrix}, \quad \langle \phi_2 \rangle = 0 \quad (1)$$

where $v \simeq 246 \text{ GeV}$. The physical spectrum of Higgs bosons consists of two scalar neutral bosons h^0 and H^0 , one pseudoscalar neutral boson A^0 and two charged Higgs H^\pm ,

$$\begin{aligned} H^0 &= \sqrt{2}[(\text{Re}\phi_1^0 - v) \cos \alpha + \text{Re}\phi_2^0 \sin \alpha], \\ h^0 &= \sqrt{2}[-(\text{Re}\phi_1^0 - v) \sin \alpha + \text{Re}\phi_2^0 \cos \alpha], \\ A^0 &= \sqrt{2}(-\text{Im}\phi_2^0). \end{aligned} \quad (2)$$

The masses of the five neutral and charged Higgs bosons and the mixing angle α are free parameters of the model. The Yukawa couplings to quarks are[2],

$$\mathcal{L}_Y^Q = \lambda_{ij}^U \bar{Q}_i \tilde{\phi}_1 U_j + \lambda_{ij}^D \bar{Q}_i \phi_1 D_j + \xi_{ij}^U \bar{Q}_i \tilde{\phi}_2 U_j + \xi_{ij}^D \bar{Q}_i \phi_2 D_j, \quad (3)$$

where the first two terms give masses of the quark mass eigenstates, and ξ_{ij}^U and ξ_{ij}^D are the 3×3 matrices which give the strength of the flavor changing neutral scalar vertices. The ξ s are all free parameters and can be constrained by the experimental data. If we neglect CP violation, the ξ s are

all real. We will use the Cheng-Sher Ansatz(CSA)[8] and let

$$\xi_{ij} \sim \frac{\sqrt{m_i m_j}}{v}.$$

And we can parametrize the Yukawa couplings as

$$\xi_{ij} = g \frac{\sqrt{m_i m_j}}{m_W} \lambda. \quad (4)$$

Comparing it with the usual gauge couplings of $SU(2) \times U(1)$, one has $\lambda = \frac{1}{\sqrt{2}}$. In our calculation we use $\lambda = \frac{1}{\sqrt{2}}$ and note that there is no theoretical bound on the coupling factor λ .

The subprocess producing $t\bar{c}(\bar{t}c)$ via gluon-gluon collisions,

$$gg \rightarrow t\bar{c}(\bar{t}c)$$

can be induced through one-loop diagrams at the lowest order, and the Feynman diagrams are drawn in figure 1(a) and figure 1(b), where the contributions from the one-loop diagrams involving neutral and charged Higgs bosons are presented, respectively. The contributions from the figures of Fig.1(b) with the charged Higgs boson in loops being replaced by W-boson, is much smaller due to the GIM suppression and Yukawa coupling. We can omitted this part in our calculation. The diagrams exchanging the two external gluon-gluon lines are not shown, but are numbered in Fig.1(a) and Fig.1(b). Fig.1(a)(1 ~ 12) and Fig. 1(b)(1 ~ 6) are the self-energy diagrams, Fig. 1(a)(13 ~ 20) and Fig. 1(b)(7 ~ 10) are the vertex correction diagrams, Fig. 1(a)(25 ~ 34) and Fig. 1(b) (13 ~ 15) are the s-channel diagrams, Fig. 1(a)(21 ~ 24) and Fig. 1(b)(11 ~ 12) are the box diagrams. Note that in the present case at one-loop level the ultraviolet divergence would be canceled automatically, if all the one-loop diagrams at the $O(m_t m_c / m_W^2)$ order in the THDM III are included. In this work, we perform the calculation in the t'Hooft-Feynman gauge.

To simplify the calculation we set $\alpha = 0$ and let all scalar bosons be degenerate, i.e., $m_{h^0} = m_{A^0} = m_{H^\pm} = M_s$ where M_s is the common scalar mass. The contribution from the coupling involving H^0 is suppressed due to $\alpha = 0$.

In the calculation for the s-channel diagrams(Fig.1.(a)(25 ~ 28)), we take into account the width effects of the h^0 and A^0 propagators. The decays of h^0 to WW and ZZ are suppressed, because of the factor $\sin \alpha$ in the $h^0 WW$ and $h^0 ZZ$ couplings, and h^0 decay to $A^0 A^0$ is also forbidden due to the case of the degenerate masses of h^0 and A^0 . Note that the pseudoscalar A^0 does not couple with gauge boson pair. Therefore only the decays of h^0 and A^0 to final states $q_i \bar{q}_j$ need to be considered, where q_i and q_j represent quarks of flavor i and j respectively. The decay width for the scalar h^0 can be written as[14]

$$\Gamma(h^0 \rightarrow q\bar{q}) = \frac{3g^2 m_{h^0}}{32\pi M_W^2} m_q \left(1 - 4m_q^2/m_{h^0}^2\right)^{3/2}$$

and

$$\Gamma(h^0 \rightarrow t\bar{c} + \bar{t}c) = \frac{3g^2 m_{h^0}}{32\pi M_W^2} \cdot 2m_t m_c \left[1 - (m_t + m_c)^2/m_{h^0}^2\right]^{3/2} \times \left[1 - (m_t - m_c)^2/m_{h^0}^2\right]^{1/2}. \quad (5)$$

The decay width for the pseudoscalar A^0 boson can be represented by exchanging exponents $3/2 \leftrightarrow 1/2$ and $m_{h^0} \leftrightarrow m_{A^0}$ in Eq.(5). When $m_t + m_c < M_s < 2m_t$, the dominant decay modes of h^0 and A^0 are $h^0, A^0 \rightarrow c\bar{c}, b\bar{b}, t\bar{c} + \bar{t}c$, whereas when $M_s > 2m_t$, the final state $t\bar{t}$ decay channel is open, and their decay widths are rather large due to the large masses of M_s and m_t .

We denote θ as the scattering angle between one of the gluons and the final top quark. Then we express all the four-momenta of the initial and final particles in the center-of-mass(CMS) by means of the total energy $\sqrt{\hat{s}}$ and the scattering angle θ . The four-momenta of top quark and charm quark are p_1 and p_2 respectively and are read

$$\begin{aligned} p_1 &= \left(E_t, \sqrt{E_t^2 - m_t^2} \sin\theta, 0, \sqrt{E_t^2 - m_t^2} \cos\theta \right), \\ p_2 &= \left(E_c, -\sqrt{E_c^2 - m_c^2} \sin\theta, 0, -\sqrt{E_c^2 - m_c^2} \cos\theta \right), \end{aligned} \quad (6)$$

where

$$E_t = \frac{1}{2} \left(\sqrt{\hat{s}} + (m_t^2 - m_c^2)/\sqrt{\hat{s}} \right), \quad E_c = \frac{1}{2} \left(\sqrt{\hat{s}} - (m_t^2 - m_c^2)/\sqrt{\hat{s}} \right). \quad (7)$$

p_3 and p_4 are the four-momenta of the initial gluons and are expressed as

$$p_3 = \left(\frac{1}{2}\sqrt{\hat{s}}, 0, 0, \frac{1}{2}\sqrt{\hat{s}} \right), \quad p_4 = \left(\frac{1}{2}\sqrt{\hat{s}}, 0, 0, -\frac{1}{2}\sqrt{\hat{s}} \right). \quad (8)$$

The corresponding matrix element for all the diagrams in figure 1(a) and figure 1(b) is written as

$$M = Tr(T^a T^b) \delta_{jl} M^{\hat{s}_1} + (f_{abc} T_{jl}^c) M^{\hat{s}_2} + (T_{jm}^a T_{ml}^b) M^{\hat{t}} + (T_{jm}^b T_{ml}^a) M^{\hat{u}} \quad (9)$$

The upper indexes $\hat{s}_1, \hat{s}_2, \hat{t}$ and \hat{u} represent the amplitudes corresponding to the s-channel diagrams Fig. 1(a) (25~28), s-channel diagrams Fig. 1(a) (29~34) and Fig. 1(b) (13~15), t-channel and u-channel diagrams in figure 1(a) and figure 1(b) respectively. The $T^a (a = 1-8)$ are the $SU(3)_c$ generators introduced by Gell-Mann and f_{abc} are the antisymmetric $SU(3)_c$ structure constants. The subscripts $j, l (j, l = 1, 2, 3)$ of T^a represent the color of final state top quark and charm quark respectively. The variables \hat{s}, \hat{t} and \hat{u} are usual Mandelstam variables in the center of mass system of gluon-gluon. Their definitions are:

$$\begin{aligned} \hat{s} &= (p_1 + p_2)^2 = (p_3 + p_4)^2, & \hat{t} &= (p_1 - p_3)^2 = (p_2 - p_4)^2, \\ \hat{u} &= (p_1 - p_4)^2 = (p_2 - p_3)^2. \end{aligned} \quad (10)$$

We collect all the explicit expressions of the amplitudes appearing in equation (9) in the appendix. The total cross section for $gg \rightarrow t\bar{c} + \bar{t}c$ can be written in the form

$$\hat{\sigma}(\hat{s}) = \frac{2}{16\pi\hat{s}^2} \int_{\hat{t}^-}^{\hat{t}^+} d\hat{t} |\bar{M}|^2 \quad (11)$$

where $|\bar{M}|^2$ is the initial spin-averaged matrix element squared and $\hat{t}^\pm = 1/2(m_t^2 + m_c^2 - \hat{s}) \pm \sqrt{E_t^2 - m_t^2} \sqrt{\hat{s}}$. The cross section for $pp \rightarrow gg \rightarrow t\bar{c} + \bar{t}c + X$ is conveniently written in terms of the

rapidities y_1 and y_2 of the two jets (final states) and their common transverse momentum p_T . Here we neglect the intrinsic transverse momentum carried by partons. It is

$$\frac{d\sigma}{dy_1 dy_2 dp_T} = \frac{\pi\tau p_T}{\hat{s}} f_g(x_1, Q^2) f_g(x_2, Q^2) \hat{\sigma}(gg \rightarrow t\bar{c} + \bar{t}c \text{ at } \hat{s} = \tau s), \quad (12)$$

where \sqrt{s} and $\sqrt{\hat{s}}$ denote the proton-proton and gluon-gluon c.m. energies respectively and $\hat{s} = s\tau$. $f_g(x_i, Q^2)$ is the distribution function of gluon in proton.

Defining

$$y^* = \frac{1}{2}(y_1 - y_2) \quad (13)$$

and

$$y_{boost} = \frac{1}{2}(y_1 + y_2). \quad (14)$$

We may write

$$\tau = \frac{4p_T^2}{s} \cosh^2 y^* \quad (15)$$

and

$$x_1 = \sqrt{\tau} e^{y_{boost}}, \quad x_2 = \sqrt{\tau} e^{-y_{boost}}. \quad (16)$$

In our numerical calculation we adopt the MRS set G parton distribution function $f_g(x_i, Q^2)$ [15] and let the factorization scale $Q^2 = \hat{s}$. The numerical calculation is carried out around the Tevatron and LHC energy ranges.

III. Numerical Results and Discussions

In the numerical calculation we take the input parameters[4] as $m_b = 4.5\text{GeV}$, $m_c = 1.35\text{GeV}$, $m_t = 175\text{GeV}$, $M_W = 80.2226\text{GeV}$, $G_F = 1.166392 \times 10^{-5}(\text{GeV})^{-2}$ and $\alpha = 1/128$. We adopt a simple one-loop formula for the running strong coupling constant α_s as

$$\alpha_s(\mu) = \frac{\alpha_s(m_Z)}{1 + \frac{33-2n_f}{6\pi} \alpha_s(m_Z) \ln\left(\frac{\mu}{m_Z}\right)}. \quad (14)$$

where $\alpha_s(m_Z) = 0.117$ and n_f is the number of active flavors at energy scale μ .

Figure 2 shows the cross sections for $gg \rightarrow t\bar{c} + \bar{t}c$ as a function of the masses of the Higgs bosons M_s . The cross sections are displayed with the three values of the gluon-gluon CMS energy 200 GeV, 400 GeV and 500 GeV respectively. Because there is no stringent bound on the Higgs bosons masses, we choose M_s in the range from 50 GeV to 800 GeV. The peak of each curve comes from s-channel resonance effects, where $M_s = m_{h^0} = m_{A^0} \sim \sqrt{\hat{s}}$. From these curves we find that the cross section can be obviously enhanced when M_s gets close to $\sqrt{\hat{s}}$.

Figure 3 shows the cross sections of $gg \rightarrow t\bar{c} + \bar{t}c$ as a function of $\sqrt{\hat{s}}$, and the three curves correspond to the M_s values 100 GeV, 250 GeV and 500 GeV, respectively. For $M_s = 100\text{GeV}$,

the effects of the widths of the Higgs bosons are not obvious, and s-channel resonance effects are suppressed, since $\sqrt{\hat{s}}$ is far beyond the Higgs boson masses M_s . Therefore the curve of its cross section is relative flat with the increasing of $\sqrt{\hat{s}}$. When $\sqrt{\hat{s}}$ approaches the value of M_s , such as $M_s = 250 GeV$ and $M_s = 500 GeV$, the cross sections will be enhanced by the s-channel resonance effects, and the width effects become stronger, since the $h^0, A^0 \rightarrow t\bar{c} + \bar{t}c$ channels are opened. In Fig.3, we can see that the curve for $M_s = 500 GeV$ shows a sharp peak around the position at $\sqrt{\hat{s}} \simeq 500 GeV$ due to the s-channel resonance effects and large width effects of h^0 and A^0 .

In figure 4 and figure 5 we show the transverse momentum spectrum of the top quark at the Tevatron and LHC energies respectively, where we assume the off-line analysis will require at least the event selection criterion of involving one isolated high p_T track with the cut of pseudorapidity $|\eta| < 2$. Again, the peaks on the curves of $M_s = 250$ and $M_s = 500$ show the s-channel resonance effects, where $M_s = m_{h^0} = m_{A^0} \sim \sqrt{\hat{s}}$.

In figure 6 and 7 we show the cross section of $pp \rightarrow gg \rightarrow t\bar{c} + \bar{t}c + X$ as a function of center-of-mass energy of electron-positron system \sqrt{s} . The cross section may reach 0.83 femtobarn when $M_s = 100 GeV$ and $\sqrt{s} = 2 TeV$ at the Tevatron and 131 femtobarn when $M_s = 100 GeV$ and $\sqrt{s} = 14 TeV$ at the LHC. For the Tevatron at 2 TeV we can expect about 4 raw events when $M_s = 100 GeV$ if we assume $5 fb^{-1}$ integrated luminosity, and for the LHC at 14 TeV we can expect about 1.3×10^4 raw events if we assume $100 fb^{-1}$ integrated luminosity. Since the cross section of this process is roughly scaled by λ^4 , if we let $\lambda \simeq 1$, the cross section will be 4 times larger. There are several potentially severe backgrounds from the SM to the signal. A top quark with a mass about $174 GeV$, decays dominantly to $t \rightarrow W^+b$. In the $t\bar{c} \rightarrow W^+b\bar{c} \rightarrow l^+\nu b\bar{c}$ detection mode, the backgrounds are mainly from $t\bar{t} \rightarrow W + jets$ and $t\bar{t} \rightarrow WWb\bar{b} \rightarrow l^+\nu q\bar{q}'b\bar{b}$ processes. The calculation shows that the cross section of top pair production will reach about $5 pb$ at the Tevatron for $\sqrt{s} = 1.8 TeV$ and about $10^2 pb$ at the LHC for $\sqrt{s} = 14 TeV$. If we use the $t\bar{c} + \bar{t}c \rightarrow lepton + jets$ detection mode, the production rate of $t\bar{c} \rightarrow W^+b\bar{c} \rightarrow l^+\nu b\bar{c}$ can reach about $0.1 fb$ at the Tevatron and $14 fb$ at the LHC, while the possible background from $t\bar{t} \rightarrow WWb\bar{b} \rightarrow l^+\nu q\bar{q}'b\bar{b}$ would be about $0.8 pb$ at the Tevatron and some dozens picobarn at the LHC. The reduction of the these backgrounds is possible through various kinematics cuts on the transverse energy, on the rapidity of jets and leptons, or involving b-tagging. Due to the very small production rate for the signal of $pp \rightarrow t\bar{c} + \bar{t}c$, it is not so easy to suppress its backgrounds. Therefore the further precise analyses are necessary to exclude these backgrounds.

In summary, from our calculation, we can conclude that if we could efficiently exclude the severe backgrounds of the $t\bar{c}(\bar{t}c)$ production signal, it would be possible at the Tevatron and the LHC that the process $pp \rightarrow gg \rightarrow t\bar{c} + \bar{t}c$ could be used to probe the flavor changing interactions in the context of the THDM III.

Acknowledgement:

This work was supported in part by the National Natural Science Foundation of China(project numbers: 19675033, 19875049), the Youth Science Foundation of the University of Science and Technology of China(USTC) and a grant from the Research Fund for the Doctoral Program of Higher Education(RFDP) of China.

Appendix

We adopt the same definitions of one-loop A, B, C and D integral functions as in Ref.[16] and the references therein. The dimension $D = 4 - \epsilon$. The integral functions are defined as

$$\begin{aligned}
A_0(m) &= -\frac{(2\pi\mu)^{4-D}}{i\pi^2} \int d^D q \frac{1}{[q^2 - m^2]}, \\
\{B_1; B_\mu; B_{\mu\nu}\}(p, m_1, m_2) &= \frac{(2\pi\mu)^{4-D}}{i\pi^2} \int d^D q \frac{\{1; q_\mu; q_{\mu\nu}\}}{[q^2 - m_1^2][(q+p)^2 - m_2^2]}, \\
\{C_0; C_\mu; C_{\mu\nu}; C_{\mu\nu\rho}\}(p_1, p_2, m_1, m_2, m_3) &= -\frac{(2\pi\mu)^{4-D}}{i\pi^2} \\
&\times \int d^D q \frac{\{1; q_\mu; q_{\mu\nu}; q_{\mu\nu\rho}\}}{[q^2 - m_1^2][(q+p_1)^2 - m_2^2][(q+p_1+p_2)^2 - m_3^2]}, \\
\{D_0; D_\mu; D_{\mu\nu}; D_{\mu\nu\rho}; D_{\mu\nu\rho\alpha}\}(p_1, p_2, p_3, m_1, m_2, m_3, m_4) &= \frac{(2\pi\mu)^{4-D}}{i\pi^2} \\
&\times \int d^D q \{1; q_\mu; q_{\mu\nu}; q_{\mu\nu\rho}; q_{\mu\nu\rho\alpha}\} \\
&\times \{[q^2 - m_1^2][(q+p_1)^2 - m_2^2][(q+p_1+p_2)^2 - m_3^2][(q+p_1+p_2+p_3)^2 - m_4^2]\}^{-1}.
\end{aligned}$$

In our calculation we take the strange quark mass $m_s = 0$. The $M^{\hat{s}_1}$ and $M^{\hat{s}_2}$ in equation (9) can be written as

$$\begin{aligned}
M^{\hat{s}_1} &= \frac{i\alpha_s^2 g^2}{16\pi^2 M_W^2} m_t \sqrt{m_t m_c} \epsilon_\mu(p_3) \epsilon_\nu(p_4) \bar{u}(p_1) \\
&\cdot \{2a_{h^0} m_t^2 (C_0 + 4C_{22} - 4C_{23}) [p_3, -p_1 - p_2, m_t, m_t, m_t] (p_1^\mu p_1^\nu + p_1^\mu p_2^\nu + p_1^\nu p_2^\mu + p_2^\mu p_2^\nu) \\
&+ 2a_{h^0} m_t^2 g^{\mu\nu} (B_0[-p_1 - p_2, m_t, m_t] - ((p_1 + p_2) \cdot p_3 C_0 + 4C_{24}) [p_3, -p_1 - p_2, m_t, m_t, m_t] \\
&+ 2ia_{A^0} m_t^2 C_0 [p_3, -p_1 - p_2, m_t, m_t, m_t] \epsilon^{\mu\nu\alpha\beta} \gamma_5 (p_1^\alpha p_3^\beta + p_2^\alpha p_3^\beta)\} v(p_2),
\end{aligned} \tag{A.1}$$

where

$$a_{h^0} = \frac{1}{\hat{s} - m_{h^0}^2 + i\Gamma_{h^0} m_{h^0}}, \quad a_{A^0} = \frac{1}{\hat{s} - m_{A^0}^2 + i\Gamma_{A^0} m_{A^0}}.$$

$$\begin{aligned}
M^{\hat{s}_2} = & \frac{i\alpha_s^2 g^2}{128\pi^2 M_W^2} m_t \sqrt{m_t m_c} \epsilon_\mu(p_3) \epsilon_\nu(p_4) \bar{u}(p_1) \\
& \cdot \{ -16m_t(C_{11} - C_{12} + C_{21} - C_{23})[-p_1, p_1 + p_2, M_s, m_t, m_t](p_1^\mu p_2^\nu - p_1^\nu p_2^\mu) \\
& + (8(2C_{24} + m_t^2(C_0 - C_{11} + C_{12} - C_{21} - C_{22} + 2C_{23}) - 2(p_1 \cdot p_2)(C_{22} + C_{23})) \\
& [-p_1, p_1 + p_2, M_s, m_t, m_t] + 4m_t^2 B_1[-p_1, m_t, M_s] - \\
& 4m_t m_c B_1[p_2, m_t, M_s] + 4m_t^2 B_1[-p_1, m_b, M_s] + \\
& 4m_t m_c B_1[p_2, m_b, M_s] + m_t^2 B_1[-p_1, m_t, M_s] \\
& - m_t m_c B_1[p_2, m_t, M_s] - m_t^2 B_1[-p_1, m_b, M_s] \\
& + m_c m_t B_1[p_2, m_b, M_s])(\gamma^\nu p_1^\mu - \gamma^\mu p_1^\nu + \gamma^\nu p_2^\mu - \gamma^\mu p_2^\nu + g^{\mu\nu} \not{p}_3) \\
& + (-4(2m_t C_{24} - 2m_t^3 C_0 + m_t(m_t^2 + 2(p_1 \cdot p_2) - 4(p_1 \cdot p_3))(C_{11} - C_{12} + C_{21} + C_{22} \\
& - 2C_{23}) + 4(p_2 \cdot p_3)(m_c C_{12} - m_t C_{22} + m_t C_{23}))[-p_1, p_1 + p_2, M_s, m_t, m_t] \\
& - (m_c m_t^2 C_0 + 2m_t C_{24} + m_t^3(C_{11} - C_{12} + C_{21} + C_{22} - 2C_{23}) + 2m_t((p_1 \cdot p_2) - \\
& 2(p_1 \cdot p_2))(C_{11} - C_{12} + C_{21} + C_{22} - 2C_{23}) + 4(p_2 \cdot p_3)(m_c C_{12} \\
& + m_t(C_{23} - C_{22}))[-p_1, p_1 + p_2, M_s, m_b, m_b] - m_t^3 B_1[-p_1, m_t, M_s] + \\
& m_t^2 m_c B_1[p_2, m_t, M_s] - m_t^3 B_1[-p_1, m_b, M_s] + (m_c m_t^2 + \\
& 2m_c p_1 \cdot p_2 - 4m_c p_1 \cdot p_3) B_1[p_2, m_b, M_s]) g^{\mu\nu} - 4m_t(C_{11} \\
& - C_{12} + C_{21} - C_{23})[-p_1, p_1 + p_2, M_s, m_b, m_b](p_1^\mu p_2^\nu - p_1^\nu p_2^\mu + \gamma_5 p_1^\mu p_2^\nu - \gamma_5 p_1^\nu p_2^\mu) \\
& + (2(2C_{24} + m_c m_t C_0 - m_t^2(C_{11} - C_{12} + C_{21} + C_{22} - 2C_{23}) - 2(p_1 \cdot p_2)(C_{22} - C_{23})) \\
& [-p_1, p_1 + p_2, M_s, m_b, m_b] + 4m_t^2 B_1[-p_1, m_b, M_s] - \\
& 4m_c m_t B_1[p_2, m_b, M_s])(\gamma^\nu p_1^\mu - \gamma^\mu p_1^\nu + \gamma^\nu p_2^\mu - \gamma^\mu p_2^\nu + g^{\mu\nu} \not{p}_3) - (m_c m_t^2 C_0 - 2m_t C_{24} \\
& - m_t^3(C_{11} - C_{12} + C_{21} + C_{22} - 2C_{23}) - 2m_t((p_1 \cdot p_2) - 2(p_1 \cdot p_2))(C_{11} - C_{12} + C_{21} \\
& + C_{22} - 2C_{23}) + 4(p_2 \cdot p_3)(m_c C_{12} - m_t(C_{23} - C_{22}))[-p_1, p_1 + p_2, M_s, m_b, m_b] \gamma_5 g^{\mu\nu} \\
& + ((4C_{24} - 2m_c m_t C_0 - 2m_t^2(C_{11} - C_{12} + C_{21} + C_{22} - 2C_{23}) + 4(p_1 \cdot p_2)(C_{23} \\
& - C_{22}))[-p_1, p_1 + p_2, M_s, m_b, m_b] + 2m_t^2 B_1[-p_1, m_b, M_s] - \\
& 2m_c m_t B_1[p_2, m_b, M_s]) \gamma_5 (\gamma^\nu p_1^\mu - \gamma^\mu p_1^\nu + \gamma^\nu p_2^\mu - \gamma^\mu p_2^\nu - g^{\mu\nu} \not{p}_3) \} v(p_2),
\end{aligned} \tag{A.2}$$

The amplitude of $M^{\hat{t}}$ can be written as

$$\begin{aligned}
M^{\hat{t}} = & \frac{i\alpha_s^2 g^2}{64\pi^2 M_W^2} m_t \sqrt{m_t m_c} \epsilon_\mu(p_3) \epsilon_\nu(p_4) \bar{u}(p_1) (f_1 p_1^\mu p_1^\nu + f_2 p_1^\mu p_2^\nu + f_3 p_1^\nu p_2^\mu + f_4 p_2^\mu p_2^\nu \\
& + f_5 \gamma^\nu p_1^\mu + f_6 \gamma^\mu p_1^\nu + f_7 \gamma^\nu p_2^\mu + f_8 \gamma^\mu p_2^\nu + f_9 \gamma^\mu \gamma^\nu + f_{10} \gamma^\nu \gamma^\mu + f_{11} \not{p}_3 p_1^\mu p_1^\nu \\
& + f_{12} \not{p}_3 p_1^\mu p_2^\nu + f_{13} \not{p}_3 p_1^\nu p_2^\mu + f_{14} \not{p}_3 p_2^\mu p_2^\nu + f_{15} \not{p}_3 \gamma^\nu p_1^\mu + f_{16} \not{p}_3 \gamma^\mu p_1^\nu + f_{17} \not{p}_3 \gamma^\nu p_2^\mu \\
& + f_{18} \not{p}_3 \gamma^\mu p_2^\nu + f_{19} \not{p}_3 \gamma^\mu \gamma^\nu + f_{20} \not{p}_3 \gamma^\nu \gamma^\mu + f'_1 \gamma_5 p_1^\mu p_1^\nu + f'_2 \gamma_5 p_1^\mu p_2^\nu + f'_3 \gamma_5 p_1^\nu p_2^\mu \\
& + f'_4 \gamma_5 p_2^\mu p_2^\nu + f'_5 \gamma_5 \gamma^\nu p_1^\mu + f'_6 \gamma_5 \gamma^\mu p_1^\nu + f'_7 \gamma_5 \gamma^\nu p_2^\mu + f'_8 \gamma_5 \gamma^\mu p_2^\nu + f'_9 \gamma_5 \gamma^\mu \gamma^\nu \\
& + f'_{10} \gamma_5 \gamma^\nu \gamma^\mu + f'_{11} \gamma_5 \not{p}_3 p_1^\mu p_1^\nu + f'_{12} \gamma_5 \not{p}_3 p_1^\mu p_2^\nu + f'_{13} \gamma_5 \not{p}_3 p_1^\nu p_2^\mu + f'_{14} \gamma_5 \not{p}_3 p_2^\mu p_2^\nu \\
& + f'_{15} \gamma_5 \not{p}_3 \gamma^\nu p_1^\mu + f'_{16} \gamma_5 \not{p}_3 \gamma^\mu p_1^\nu + f'_{17} \gamma_5 \not{p}_3 \gamma^\nu p_2^\mu + f'_{18} \gamma_5 \not{p}_3 \gamma^\mu p_2^\nu \\
& + f'_{19} \gamma_5 \not{p}_3 \gamma^\mu \gamma^\nu + f'_{20} \gamma_5 \not{p}_3 \gamma^\nu \gamma^\mu) v(p_2),
\end{aligned} \tag{A.3}$$

where the f_i 's and f'_i 's are expressed explicitly as,

$$f'_1 = 4(m_c(D_{38} - D_{310}) + m_t(D_{32} - D_{36}))[p_3, -p_1, -p_2, m_b, m_b, M_s, m_b] \tag{A.4}$$

$$f_1 = f'_1(m_t \rightarrow -m_t) + 8m_t(D_{11} - D_{12} + D_{21} - D_{24} - D_{25} + D_{26})[p_1, -p_3, -p_4, M_s, m_t, m_t, m_t] \quad (\text{A.5})$$

$$f'_2 = 4a_1(m_c C_{22} - m_t C_{12} - m_t C_{23})[-p_4, p_2, m_b, m_b, M_s] + 4(m_c(D_{39} - D_{310}) - m_t(D_{22} - D_{26} + D_{36} - D_{38}))[p_3, -p_1, -p_2, m_b, m_b, M_s, m_b] \quad (\text{A.6})$$

$$f_2 = f'_2(m_t \rightarrow -m_t) + 8a_1 m_t C_{11}[-p_2, p_4, M_s, m_t, m_t] - 8m_t(D_{12} + D_{24} - D_{26})[p_1, -p_3, -p_4, M_s, m_t, m_t, m_t] \quad (\text{A.7})$$

$$f'_3 = 4(m_c(D_{39} - D_{37}) - m_t(D_{310} - D_{38}))[p_3, -p_1, -p_2, m_b, m_b, M_s, m_b] \quad (\text{A.8})$$

$$f_3 = f'_3(m_t \rightarrow -m_t) - 8m_t(D_{25} - D_{26})[p_1, -p_3, -p_4, M_s, m_t, m_t, m_t] \quad (\text{A.9})$$

$$f'_4 = 4(m_c(D_{33} - D_{37}) + m_t(D_{23} - D_{26} - D_{310} + D_{39}))[p_3, -p_1, -p_2, m_b, m_b, M_s, m_b] \quad (\text{A.10})$$

$$f_4 = f'_4(m_t \rightarrow -m_t) + 8m_t D_{26}[p_1, -p_3, -p_4, M_s, m_t, m_t, m_t] \quad (\text{A.11})$$

$$\begin{aligned} f'_5 = & -2a_2 a_3 m_t^2 B_1[-p_1, m_b, M_s] - 2a_1 a_2 (m_t^2 - 2(p_1 \cdot p_3)) B_1[-p_1 + p_3, m_b, M_s] \\ & - 2a_1 a_3 m_c m_t B_1[p_2, m_b, M_s] + 2a_2 (m_c m_t (C_0 + 2C_{11} + C_{21}) - 2C_{24})[p_1, -p_3, M_s, m_t, m_t] \\ & + 2a_1 (-2C_{24} - m_b^2 C_0 + m_c^2 (C_{22} - 2C_{23}) - m_c m_t C_{12} + m_t^2 (C_{11} + C_{21})) \\ & + 2(p_1 \cdot p_2 - p_2 \cdot p_3) (C_{11} - C_{12} + C_{21} - C_{23}) \\ & - 2(p_1 \cdot p_3) (C_{11} + C_{21})[-p_4, p_2, m_b, m_b, M_s] \\ & + 2(2D_{27} + 2D_{312} + m_b^2 D_0 - m_c^2 D_{23} - m_c m_t (D_{22} - D_{26}) \\ & + 2(p_2 \cdot p_3) (D_{25} - D_{26}))[p_3, -p_1, -p_2, m_b, m_b, M_s, m_b] \end{aligned} \quad (\text{A.12})$$

$$\begin{aligned} f_5 = & f'_5(m_t \rightarrow -m_t) + 4a_2 a_3 m_t^2 B_0[-p_1, m_t, M_s] \\ & + 4a_1 a_2 m_t^2 B_0[-p_1 + p_3, m_t, M_s] - 4a_1 a_3 m_t^2 B_0[p_2, m_t, M_s] \\ & - 4a_2 m_t^2 (C_0 + C_{11})[p_1, -p_3, M_s, m_t, m_t] - 4a_1 m_t^2 [-p_2, p_4, M_s, m_t, m_t] \\ & + 4m_t^2 (D_0 + D_{11} - D_{13})[p_1, -p_3, -p_4, M_s, m_t, m_t, m_t] \end{aligned} \quad (\text{A.13})$$

$$\begin{aligned} f'_6 = & 2(4(D_{311} - D_{312}) + m_b^2 (D_{11} - D_{12}) - m_c^2 (D_{37} - D_{39}) \\ & + m_t^2 (D_{32} - D_{36}) + 2(p_1 \cdot p_2) (D_{38} - D_{310}) - 2(p_1 \cdot p_3) (D_{22} - D_{24} - D_{34} + D_{36}) \\ & + 2(p_1 \cdot p_2) (D_{35} - D_{310}))[p_3, -p_1, -p_2, m_b, m_b, M_s, m_b] \end{aligned} \quad (\text{A.14})$$

$$f_6 = f'_6 \quad (\text{A.15})$$

$$f'_7 = 2(-4D_{313} - m_b^2 D_{13} + m_c^2 D_{33} + m_c m_t D_{23} + m_t^2 (D_{26} + D_{38}) + 2(p_1 \cdot p_2)(D_{23} + D_{39}) - 2(p_1 \cdot p_3)(D_{25} + D_{310} + D_{23} + D_{37}))[p_3, -p_1, -p_2, m_b, m_b, M_s, m_b] \quad (A.16)$$

$$f_7 = f'_7(m_t \rightarrow -m_t) - 4m_t^2 D_{13}[p_1, -p_3, -p_4, M_s, m_t, m_t, m_t] \quad (A.17)$$

$$f'_8 = -4a_1(p_1 \cdot p_3)(C_{12} + C_{23})[-p_4, p_2, m_b, m_b, M_s] + 2(2(D_{27} + 2D_{311} + D_{313}) + m_b^2(D_0 + D_{11}) - m_c^2(D_{23} + D_{37}) - m_t^2(D_{22} + D_{36}))[p_3, -p_1, -p_2, m_b, m_b, M_s, m_b] - (p_1 \cdot p_2)(D_{26} + D_{310}) + 2(p_1 \cdot p_3)(D_{12} - D_{13} + 4D_{24} - D_{26} + D_{34}) + 2(p_2 \cdot p_3)(D_{25} + D_{35}))[p_3, -p_1, -p_2, m_b, m_b, M_s, m_b] \quad (A.18)$$

$$f_8 = f'_8 \quad (A.19)$$

$$f'_9 = -a_2 a_3 m_t^3 B_1[-p_1, m_b, M_s] + 2a_1 a_2 m_c (p_1 \cdot p_3) B_1[-p_1 + p_3, m_b, M_s] - a_2 m_t (2C_{24} - m_t^2(C_0 + 2C_{11} + C_{21}) + 2(p_1 \cdot p_3)(C_0 + C_{11} + C_{12} + C_{23}))[p_1, -p_3, M_s, m_t, m_t] - 2a_1 m_c (p_1 \cdot p_3) C_{12}[-p_4, p_2, m_b, m_b, M_s] + (4m_c(D_{313} + m_b^2 D_{13} - m_c^2 D_{33}) + m_t(2D_{27} + 4D_{312} + m_b^2(D_0 + D_{12}) - m_c^2(D_{23} + D_{39}) - m_t(m_c D_{38} - m_t D_{22} - m_t D_{32})) - 2(p_1 \cdot p_2)(m_c D_{39} + m_t D_{26} + m_t D_{38}) + 2(p_1 \cdot p_3)(m_c D_{12} - m_c D_{13} + m_c D_{310} + m_t D_{24} + m_t D_{36}) + 2(p_2 \cdot p_3)(m_c D_{37} + m_t D_{25} + m_t D_{310}))[p_3, -p_1, -p_2, m_b, m_b, M_s, m_b] \quad (A.20)$$

$$f_9 = f'_9(m_t \rightarrow -m_t) - 2a_2 a_3 m_t^3 B_0[-p_1, m_t, M_s] - 4a_1 a_2 m_t (p_1 \cdot p_3) B_0[-p_1 + p_3, m_t, M_s] + 4a_2 m_t (p_1 \cdot p_3) C_0[p_1, -p_3, M_s, m_t, m_t] + 4a_1 m_t (p_1 \cdot p_3) C_0[-p_2, p_4, M_s, m_t, m_t] + 4m_t(D_{27} + D_{311} - D_{313})[p_1, -p_3, -p_4, M_s, m_t, m_t, m_t] \quad (A.21)$$

$$f'_{10} = -2(m_c D_{313} + m_t D_{312})[p_3, -p_1, -p_2, m_b, m_b, M_s, m_b] \quad (A.22)$$

$$f_{10} = f'_{10}(m_t \rightarrow -m_t) - 4m_t D_{27}[p_1, -p_3, -p_4, M_s, m_t, m_t, m_t] \quad (A.23)$$

$$f'_{11} = 4(D_{22} - D_{24} - D_{34} + D_{36})[p_3, -p_1, -p_2, m_b, m_b, M_s, m_b] \quad (A.24)$$

$$f_{11} = f'_{11} \quad (A.25)$$

$$f'_{12} = 4(D_{13} - D_{12} - 2D_{24} + 2D_{26} + D_{310} - D_{34})[p_3, -p_1, -p_2, m_b, m_b, M_s, m_b] \quad (A.26)$$

$$f_{12} = f'_{12} \quad (A.27)$$

$$f'_{13} \quad (A.28)$$

$$f_{13} = f'_{13} \quad (A.29)$$

$$f'_{14} = 4(D_{23} - D_{25} - D_{35} + D_{37})[p_3, -p_1, -p_2, m_b, m_b, M_s, m_b] \quad (A.30)$$

$$f_{14} = f'_{14} \quad (A.31)$$

$$f'_{15} = -2a_2 m_t (C_{11} - C_{12} + C_{21} - C_{23})[p_1, -p_3, M_s, m_t, m_t] \\ + 2(m_c(D_{13} - D_{12} + D_{26}) + m_t(D_{22} - D_{24}))[p_3, -p_1, -p_2, m_b, m_b, M_s, m_b] \quad (A.32)$$

$$f_{15} = f'_{15}(m_t \rightarrow -m_t) + 4a_2 m_t C_{11}[p_1, -p_3, M_s, m_t, m_t] \\ - 4m_t(D_{11} - D_{13})[p_1, -p_3, -p_4, M_s, m_t, m_t, m_t] \quad (A.33)$$

$$f'_{16} = 2(m_c(D_{25} - D_{26}) - m_t(D_{22} - D_{24}))[p_3, -p_1, -p_2, m_b, m_b, M_s, m_b] \quad (A.34)$$

$$f_{16} = f'_{16}(m_t \rightarrow -m_t) + 4m_t(D_{11} - D_{12})[p_1, -p_3, -p_4, M_s, m_t, m_t, m_t] \quad (A.35)$$

$$f'_{17} = 2(m_c D_{23} - m_t(D_{25} - D_{26}))[p_3, -p_1, -p_2, m_b, m_b, M_s, m_b] \quad (A.36)$$

$$f_{17} = f'_{17}(m_t \rightarrow -m_t) + 4m_t D_{13}[p_1, -p_3, -p_4, M_s, m_t, m_t, m_t] \quad (A.37)$$

$$f'_{18} = 2a_1(m_c C_{22} - m_t C_{12} - m_t C_{23})[-p_4, p_2, m_b, m_b, M_s] \\ + 2(m_c(D_{25} - D_{23}) + m_t(D_{12} - D_{13} + D_{24} - D_{26}))[p_3, -p_1, -p_2, m_b, m_b, M_s, m_b] \quad (A.38)$$

$$f_{18} = f'_{18}(m_t \rightarrow -m_t) + 4a_1 m_t C_{11}[-p_2, p_4, M_s, m_t, m_t] \\ - 4m_t D_{12}[p_1, -p_3, -p_4, M_s, m_t, m_t, m_t] \quad (A.39)$$

$$\begin{aligned}
f'_{19} = & -a_2 a_3 m_t^2 B_1[-p_1, m_b, M_s] \\
& -a_1 a_2 (m_t^2 - 2(p_1 \cdot p_3)) B_1[-p_1 + p_3, m_b, M_s] \\
& -a_1 a_3 m_c m_t B_1[p_2, m_b, M_s] - a_2 (2C_{24} - m_t(m_c C_0 + m_t C_{11} \\
& + m_t C_{21}) + 2(C_{12} + C_{23})(p_1 \cdot p_3)) [p_1, -p_3, M_s, m_t, m_t] \\
& + a_1 (-2C_{24} - m_b^2 C_0 + m_c^2 (C_{22} - 2C_{23}) - m_c m_t C_{12} \\
& + m_t^2 (C_{11} + C_{21}) + 2((p_1 \cdot p_2) - (p_2 \cdot p_3))(C_{11} - C_{12} + C_{21} - C_{23}) \\
& - 2(p_1 \cdot p_3)(C_{11} + C_{21})) [-p_4, p_2, m_b, m_b, M_s] \\
& + (4(D_{27} + D_{311}) + 2m_b^2 (D_0 + D_{11}) - 2m_c^2 (D_{23} + D_{37}) - D_{13} m_c m_t \\
& - m_t^2 (D_{12} + D_{22} + D_{36}) - 2(p_1 \cdot p_2)(D_{12} + 2D_{26} + D_{310}) + 2(p_1 \cdot p_3)(D_{12} \\
& + 2D_{24} + D_{34}) + 2(p_2 \cdot p_3)(D_{13} + 2D_{25} + D_{35})) [p_3, -p_1, -p_2, m_b, m_b, M_s, m_b]
\end{aligned} \tag{A.40}$$

$$\begin{aligned}
f_{19} = & f'_{19}(m_t \rightarrow -m_t) + 2a_2 a_3 m_t^2 B_0[-p_1, m_t, M_s] \\
& + 2a_1 a_2 m_t^2 B_0[-p_1 + p_3, m_t, M_s] - 2a_1 a_2 m_t^2 B_0[p_2, m_t, M_s] \\
& - 2a_2 m_t^2 C_0[p_1, -p_3, M_s, m_t, m_t] - 2a_1 m_t^2 C_0[-p_2, p_4, M_s, m_t, m_t] \\
& + 2m_t^2 D_0[p_1, -p_3, -p_4, M_s, m_t, m_t, m_t]
\end{aligned} \tag{A.41}$$

$$f'_{20} = -2D_{311}[p_3, -p_1, -p_2, m_b, m_b, M_s, m_b] \tag{A.42}$$

$$f_{20} = f'_{20} \tag{A.43}$$

where

$$a_1 = \frac{1}{\hat{t} - m_t^2}, \quad a_2 = \frac{1}{\hat{t} - m_c^2} \quad \text{and} \quad a_3 = \frac{1}{m_t^2 - m_c^2}.$$

$$M^{\hat{u}} = M^{\hat{t}} \quad (p_3 \leftrightarrow p_4, \quad \mu \leftrightarrow \nu, \hat{t} \leftrightarrow \hat{u}) \tag{A.44}$$

References

- [1] S. Glashow and S. Weinberg, Phys. Rev. **D15**, 1958(1977) ; T. P. Cheng and M. Sher, *ibid.* **D35**, 3484(1987) ; M. Sher and Y. Yuan, *ibid.* **44**, 1461(1991).
- [2] M. Luke and M. J. Savage, Phys. Lett. **B207**, 387(1993).
- [3] S. L. Glashow and S. Weinberg, Phys. Rev. **D15**, 1958(1977).
- [4] C. Caso, G. Conforto et al., 'Review of Particle Physics', Euro. Phys. J. **C3**, (1998)1.
- [5] F. Abe et al., CDF Collaboration, Phys. Rev. Lett. **80**, 2779(1998); F. Abe et al., CDF Collaboration, Phys. Rev. Lett. **80**, 2767(1998); S. Abachi et al., The D0 Collaboration, Phys. Rev. Lett. **79**, 1197(1997).

- [6] A. Antaramian, L. J. Hall and A. Rasin, Phys. Rev. Lett. **69**, 1871(1992).
- [7] D. Chang, W. S. Hou and W. Y. Keung, CERN preprint CERN-TH. 6795/93(1993).
- [8] T. P. Cheng and M. Sher, Phys. Rev. **D35**, 3484(1987); M. Sher and Y. Yuan, *ibid.* **44**, 1461(1991)
- [9] W. S. Hou, Phys. Lett. **B 296**, 179(1992); D. Chang, W. S. Hou and W. Y. Keung, Phys. Rev. **D48**, 217(1993).
- [10] David Atwood et al. Phys. Rev. **D53**, 1199(1996).
- [11] Jiang Yi, Zhou Mian-Lai, Ma Wen-Gan, Han Liang, Zhou Hong and Han Meng, Phys. Rev. **D57**, 4343(1998);
- [12] K. J. Abraham et al., Phys. Lett. **B419**, 381(1998).
- [13] Wei-Shu Hou and Guey-Lin Lin, Phys. Lett. **B379**, 261(1996).
- [14] W. S. Hou, Phys. Lett. **B 296**, 179(1992).
- [15] A.D. Martin, W.J. Stirling and R.G. Roberts, Phys. Lett. **B354**, 155(1995).
- [16] Kniehl B. A., Phys. Rep. 240(1994)211 and references therein.

Figure Captions

Fig.1(a)(b) The Feynman diagrams of the subprocess $gg \rightarrow t\bar{c}$.

Fig.2 Total cross sections of the subprocess $gg \rightarrow t\bar{c} + \bar{t}c$ as function of M_s . The solid curve is for $\sqrt{\hat{s}} = 200 GeV$, the dashed curve is for $\sqrt{\hat{s}} = 400 GeV$ and the dotted curve is for $\sqrt{\hat{s}} = 500 GeV$.

Fig.3 Total cross sections of the subprocess $gg \rightarrow t\bar{c} + \bar{t}c$ as function of $\sqrt{\hat{s}}$. The solid curve is for $M_s = 100 GeV$, the dashed curve is for $M_s = 250 GeV$ and the dotted curve is for $M_s = 500 GeV$.

Fig.4 The transverse momentum spectrum of top quark for the Tevatron at 2 TeV. The solid curve is for $M_s = 100 GeV$, the dashed curve is for $M_s = 250 GeV$ and the dotted curve is for $M_s = 500 GeV$.

Fig.5 The transverse momentum spectrum of top quark for the LHC at 14 TeV. The solid curve is for $M_s = 100 GeV$, the dashed curve is for $M_s = 250 GeV$ and the dotted curve is for $M_s = 500 GeV$.

Fig.6 Total cross sections of the process $pp \rightarrow gg \rightarrow t\bar{c} + \bar{t}c$ as function of \sqrt{s} at the Tevatron. The solid curve is for $M_s = 100 GeV$, the dashed curve is for $M_s = 250 GeV$ and the dotted curve is for $M_s = 500 GeV$.

Fig.7 Total cross sections of the process $pp \rightarrow gg \rightarrow t\bar{c} + \bar{t}c$ as function of \sqrt{s} at the LHC. The solid curve is for $M_s = 100 GeV$, the dashed curve is for $M_s = 250 GeV$ and the dotted curve is for $M_s = 500 GeV$.

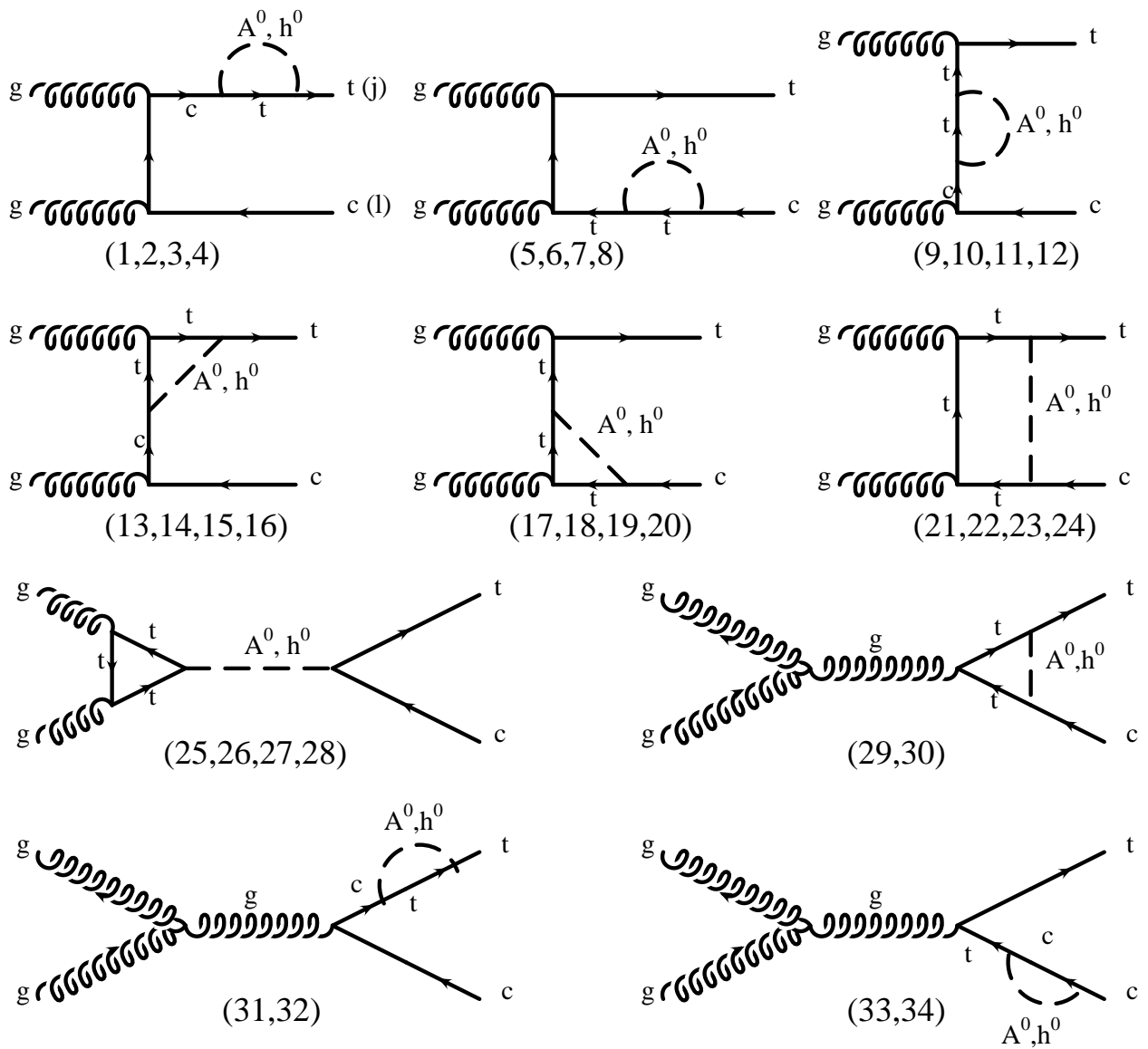


Fig.1 (a)

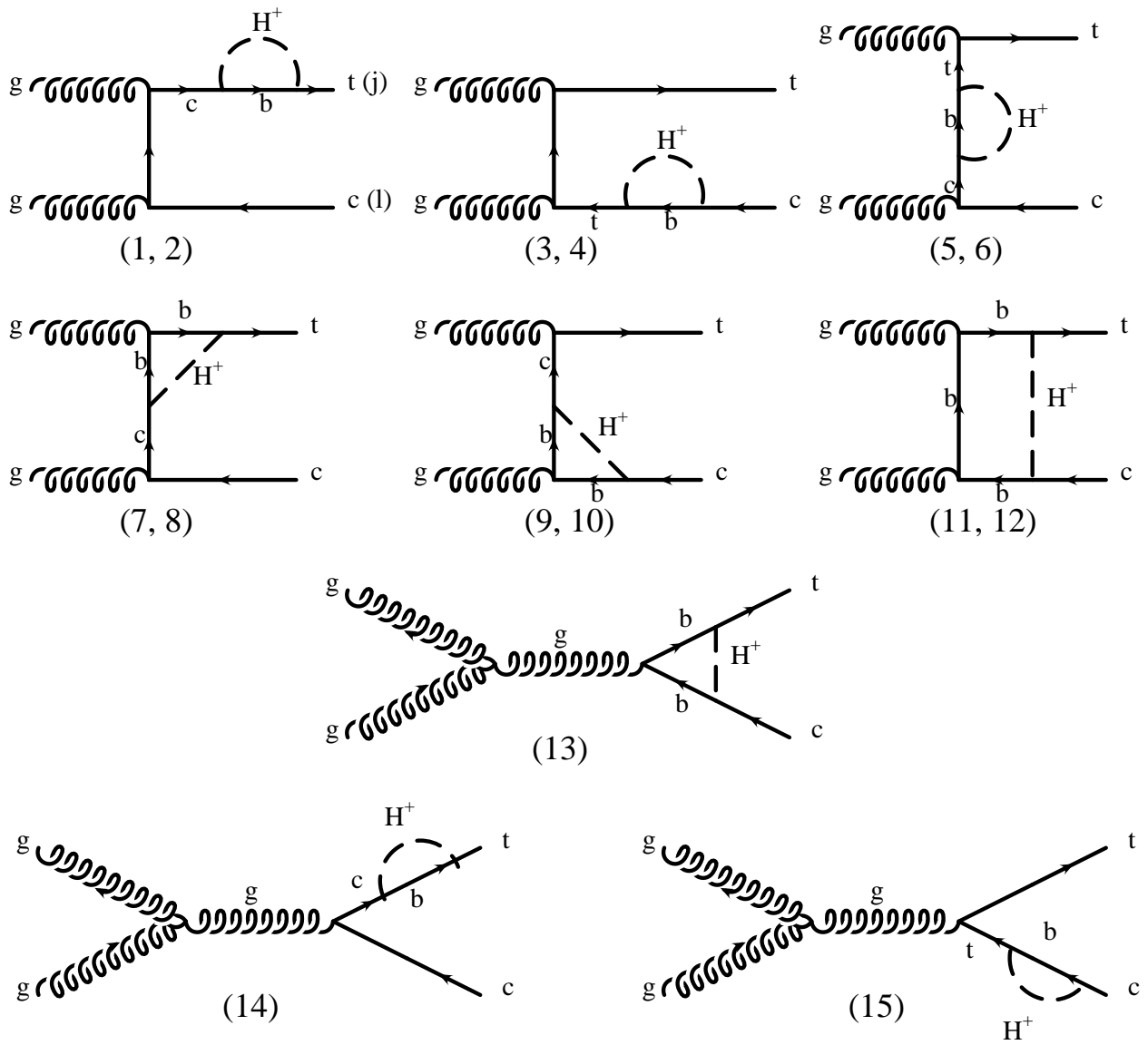


Fig.1 (b)

Fig.(2)

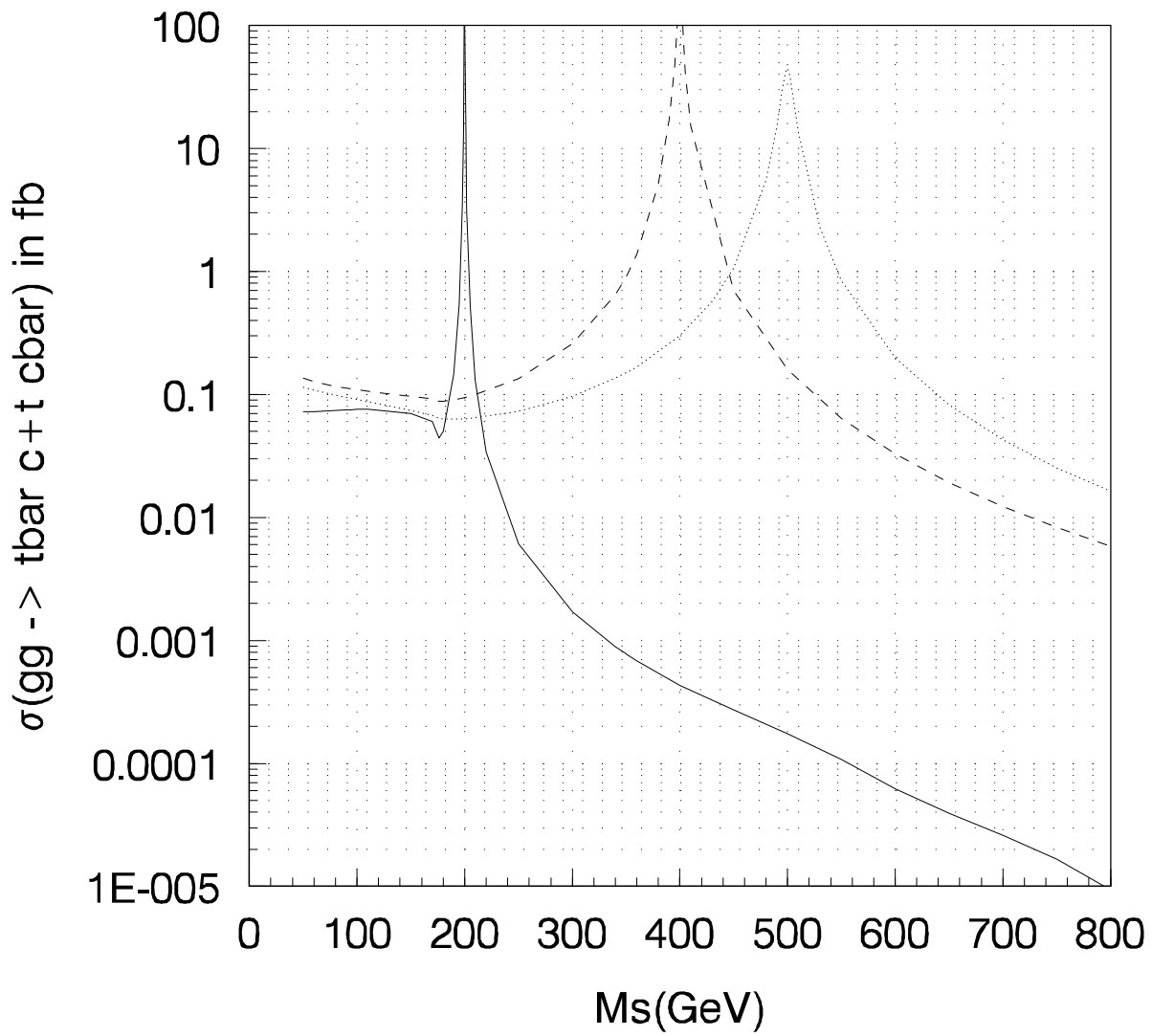


Fig.(3)

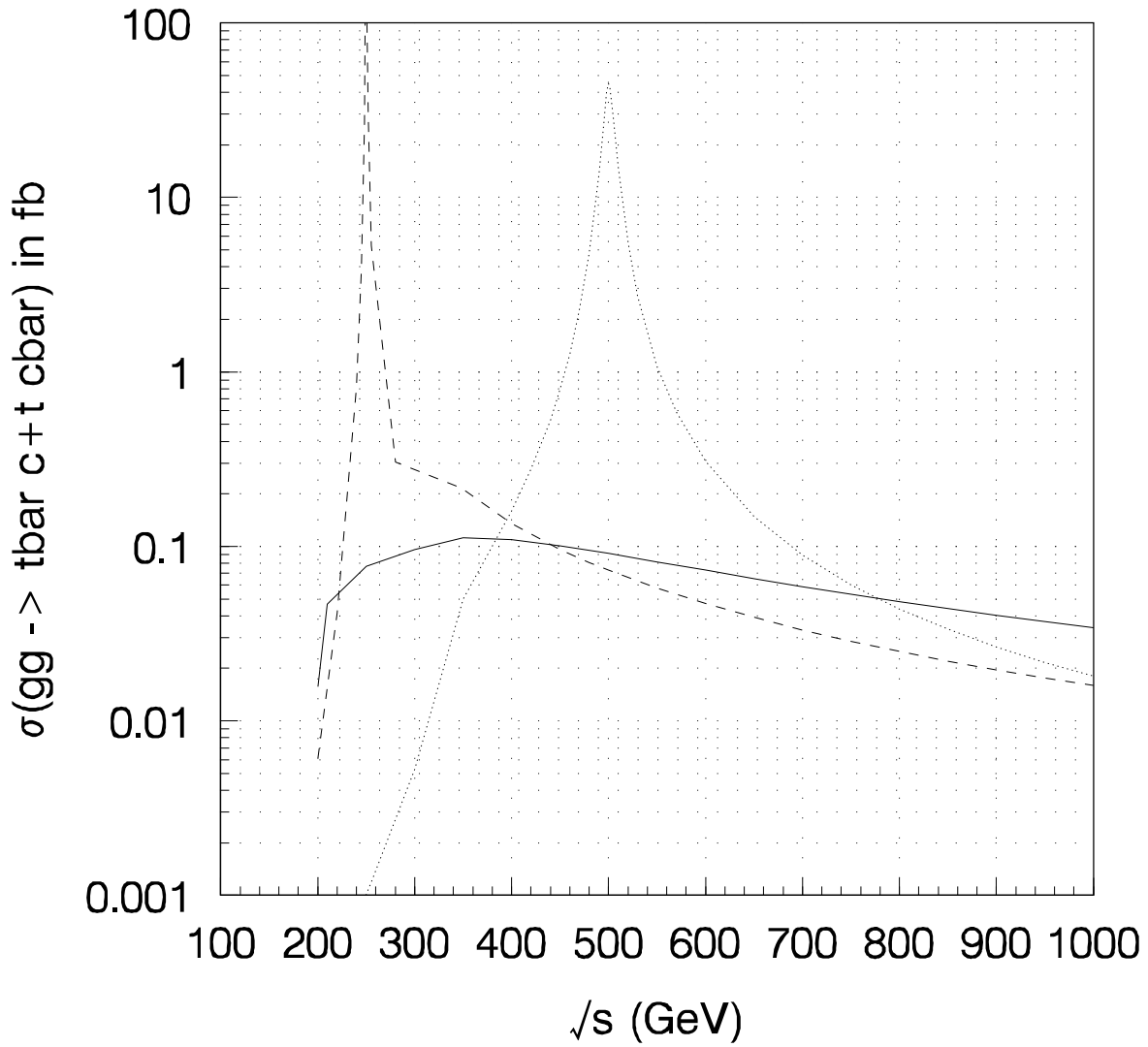


Fig.(4)

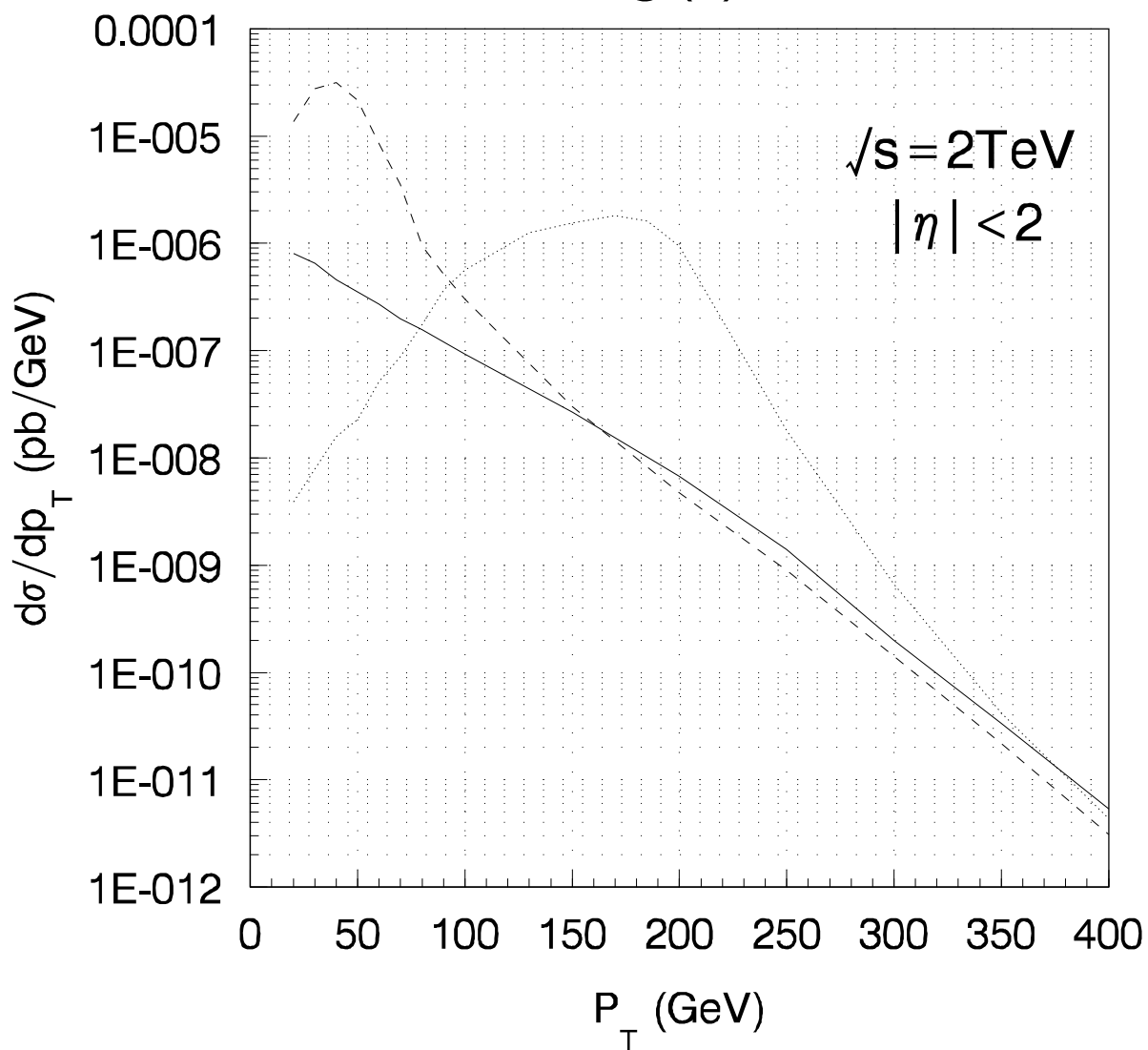


Fig.(5)

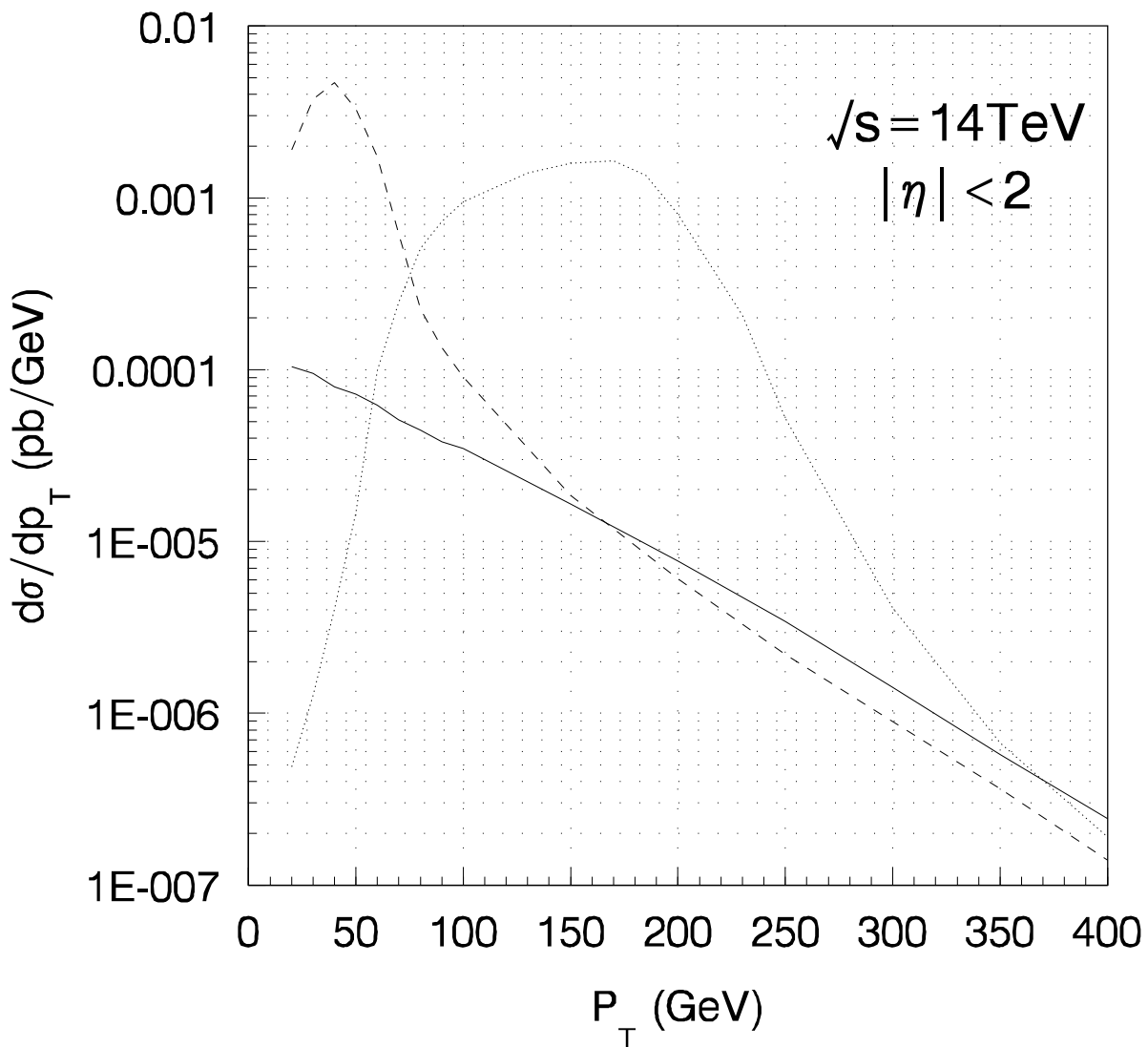


Fig.(6)

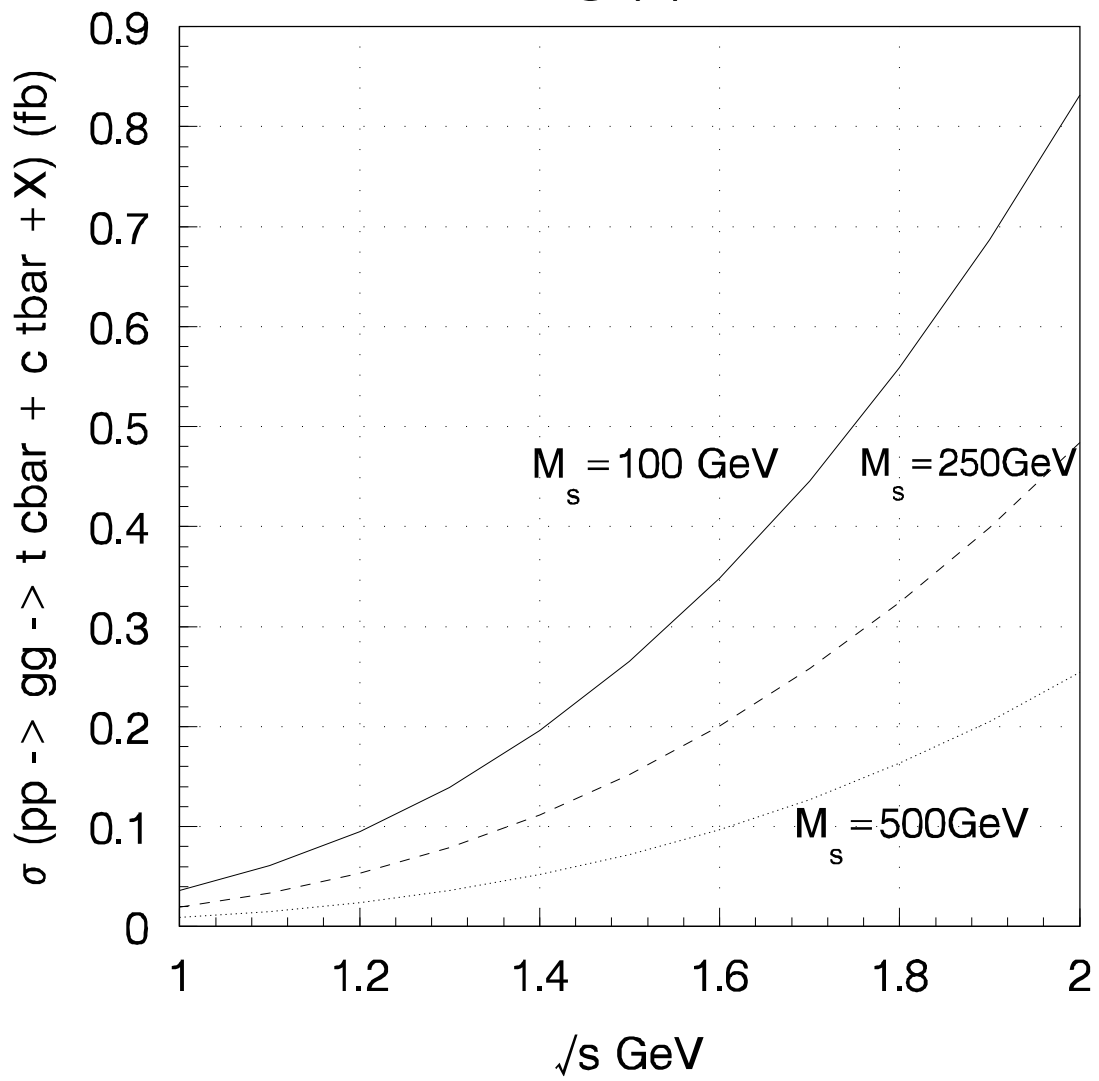


Fig.(7)

